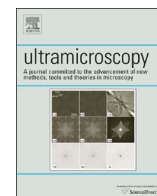




Contents lists available at ScienceDirect

Ultramicroscopy

journal homepage: www.elsevier.com/locate/ultramic

Single-atom detection of light elements: Imaging or spectroscopy?

Ryosuke Senga, Kazu Suenaga*

Nano-Materials Research Institute, National Institute of Advanced Industrial Science and Technology (AIST), Tsukuba 305-8565, Japan

ARTICLE INFO

Keywords:

One-dimensional material
Light element
Single-atom detection
Low voltage
STEM-EELS

ABSTRACT

Single-atom imaging and spectroscopy at a lower accelerating voltage (~60 kV) has been largely facilitated by the development of aberration correctors for transmission electron microscopy (TEM)/ scanning TEM (STEM). Such a STEM condition will reduce beam damage and has therefore been demonstrated capable of detecting individual atoms of light elements including B, C, and N in mono-layered materials. However, other light elements such as Li, O, or F are still difficult to visualise as individual atoms by using conventional STEM/TEM imaging because their extremely weak contrast can be often smeared out by the other atoms nearby. In this paper, we demonstrate the successful detection of these 'hardly visible' atoms in the spectroscopy mode.

1. Introduction

Since Dalton's atomic theory, scientists have dreamed of the direct 'imaging' and 'identification' of individual atoms. With respect to 'imaging', single heavy atoms on a thin C film were observed by scanning electron microscopy by Crewe in 1970 [1]. Then, owing to several important developments in aberration correction [2–5], atomically resolved crystal images were successfully obtained by both transmission electron microscopy (TEM) [6] and scanning TEM (STEM) [7–9]. On the other hand, single-atom 'identification' by electron energy-loss spectroscopy (EELS) was theoretically predicted in the 1970s [10]. However, experimental verification had been lacking until the 1990s because of the absence of ideal samples. The possibility of single-atom detection by EELS was discussed by Krivanek et al. in 1991 by demonstrating EELS quantification for small Th clusters on a thin C film [11]. However, the unambiguous demonstration of single-atom identification was never carried out until 2000 when Gd atoms inside fullerene cages were clearly imaged in an EELS map [12].

Thereafter, STEM-EELS has served as the most powerful tool for material characterisations at the atomic level [13–16]. In particular, since a ~1 Å probe at lower accelerating voltages (30–60 kV) is now routinely available with the latest aberration correctors [17–19], nanomaterials such as graphene or carbon nanotubes, which are easily damaged by electron beams at higher acceleration voltages (> 80–120 kV), can be also observed at the atomic level [20–23]. In addition, EELS is capable of examining the detailed chemical states of probed atoms using energy-loss near-edge fine structures (ELNESs). For instance, the ELNES of the C *K-edge*, which has rich information regarding its chemical bonds, can discriminate singly, doubly, and

triply coordinated carbon atoms at the graphene edge with atomic resolution [23]. Moreover, the spin states of single transition-metal atoms (Fe, Cr) doped in a graphene lattice have been also successfully extracted using a white line analysis [24].

In such experiments, the operators usually start by finding the typical places with specific atomic configurations of interest such as defects in materials by annular dark-field (ADF) images and then perform spectroscopy at the target atom. This means that the STEM-EELS analysis so far is based on the fact that the targeted atoms are 'visible' according to the ADF images. Thus, the following question arises: if atoms are 'invisible' according to the ADF images, how can we find them?

Since the ADF contrast is related to the cross section of elastic scattering and proportional to the square of the atomic number, the location of heavier atoms in a matrix of lighter elements can be straightforwardly recognised by ADF images. In the other case where the target materials are only composed of elements which are located close to each other in the periodic table, e.g. single N ($Z=7$) or O ($Z=8$) atoms doped in a graphene lattice (carbon: $Z=6$), even light atoms can be identified by means of a quantitative analysis of the ADF contrast recorded under the proper conditions (middle-angular ADF (MAADF) conditions in a typical case) [21]. However, for a more complex system such as a crystal with a wide variety of light and heavy elements, the ADF images are not fully adequate for identifying elements atom-by-atom because no specific elemental signals can be obtained. In particular, extremely light atoms such as Li or H are quite difficult to visualise as single atoms when they are located in the vicinities of some other heavier elements because of their significantly higher scattering power, which could smear out the contrast of the light elements.

* Corresponding author.

E-mail address: kazu@aist.go.jp (K. Suenaga).<http://dx.doi.org/10.1016/j.ultramic.2016.12.007>Received 5 October 2016; Received in revised form 17 November 2016; Accepted 8 December 2016
0304-3991/ © 2016 Elsevier B.V. All rights reserved.

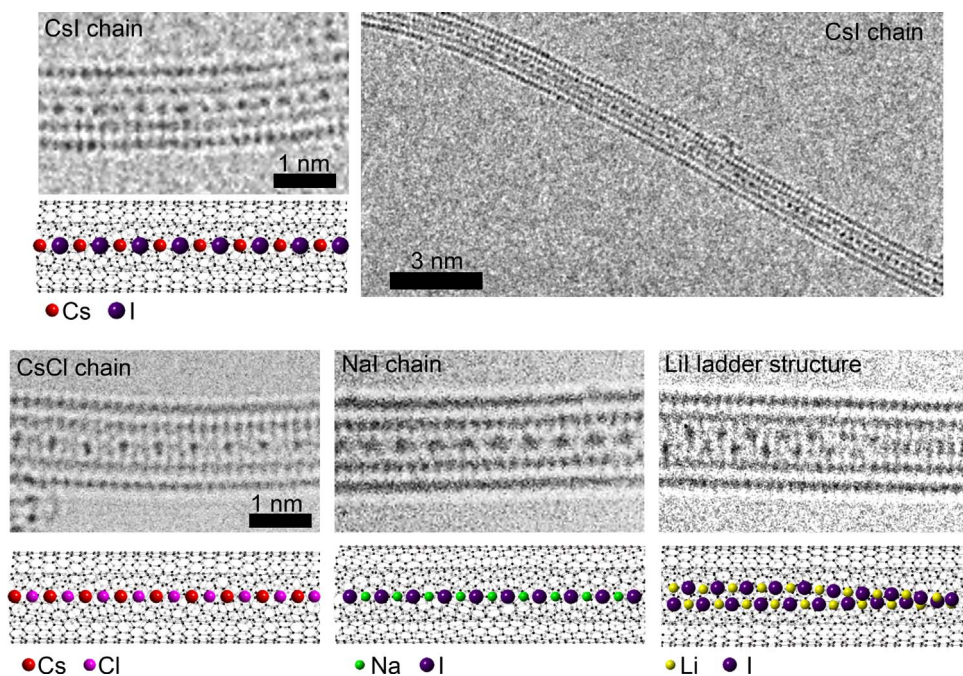


Fig. 1. Examples of ‘visible’ and ‘hardly visible’ atoms in conventional TEM images of one-dimensional atomic chains (operated at 60 kV). The upper panels show typical TEM images of a CsI atomic chain inside a DWNT. The Cs and I atoms are alternatively aligned in a row. In this case, both elements are clearly visualised as darker spots between four carbon nanotube walls. The bottom panels show TEM images of CsCl, NaI, and LiI atomic chains inside DWNTs (from left to right). Heavier atoms (Cs and I) presumably show strong contrast, while lighter atoms (Cl, Na, and Li) cannot be identified from the contrast. Note that these light atoms show weak contrast in relatively under focused TEM images when they are almost immobile in a confined space (Supplementary information). The TEM images were taken at 60 kV.

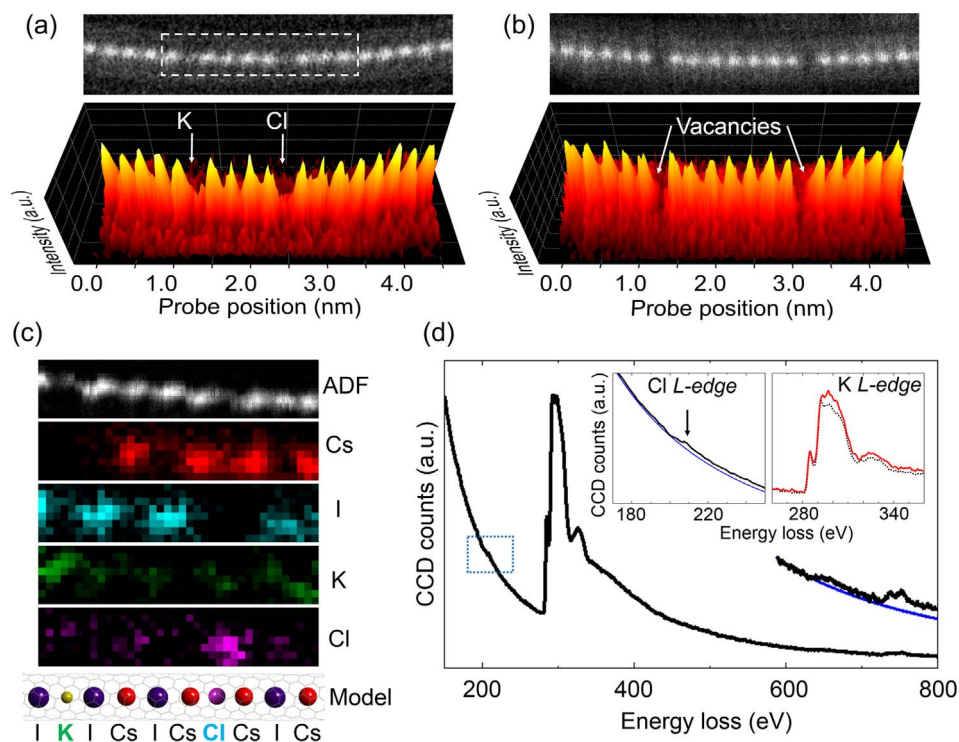


Fig. 2. Detection of single dopant atoms and mono-vacancies in CsI atomic chains co-doped with K and Cl. STEM images (top) and intensity profile maps of the ADF contrast (bottom) for CsI atomic chains involving (a) K and Cl substitutions and (b) two vacancies. (c) EELS chemical map constructed from the EELS spectra shown in (d) collected from the chain in (a) around the dopants. The STEM images were taken at 60 kV. A principal component analysis (PCA) was performed to create the elemental map in (c), although the spectra in (d) are not processed.

Although single atomic columns of light elements in thick crystals were visualised by annular bright-field (ABF) contrast [25], several tens of identical atoms contribute to the ABF column images through a channelling effect. If the target is only a single atom thick, the ABF

contrast is not advantageous over the ADF because no channelling effect is expected.

Therefore, another approach is needed to identify the location of such single invisible atoms of light elements instead of ADF/ABF

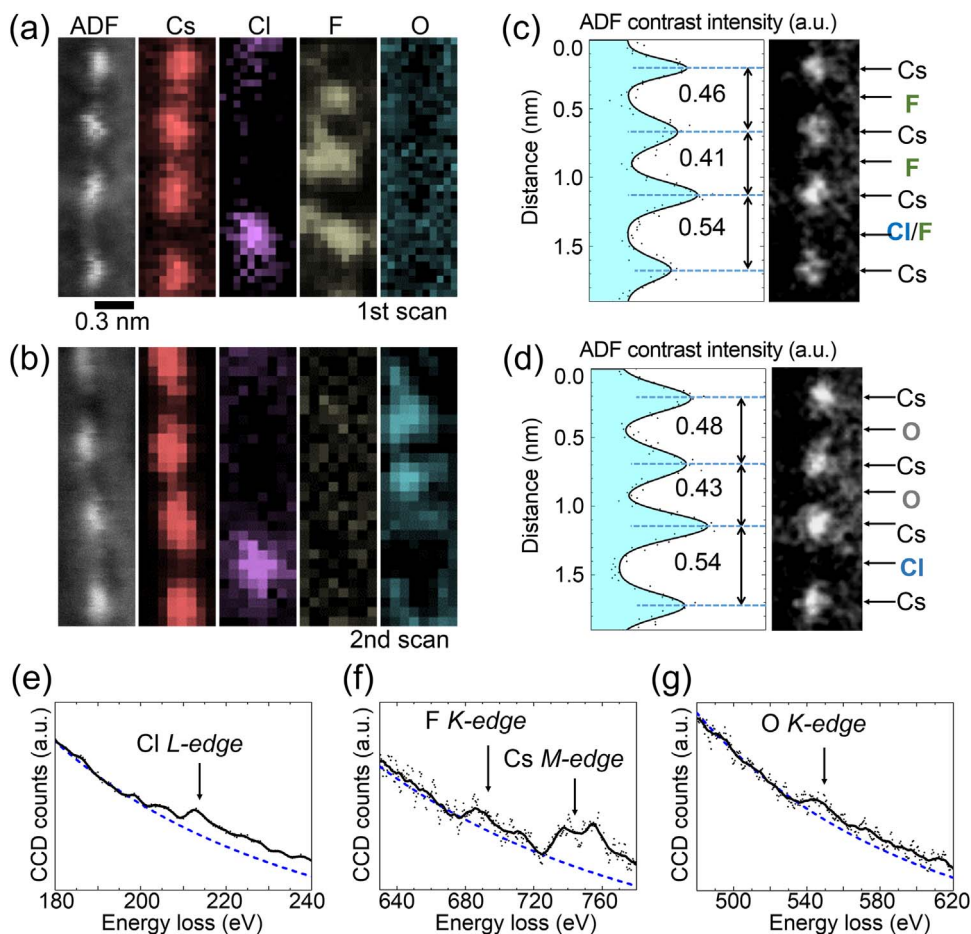


Fig. 3. Chemical evolutions of an atomic chain of CsF with an impurity of Cl atom. (a, b) ADF images and EELS elemental maps for Cs, Cl, F, and O for the first and second scans, respectively. (c, d) Line profiles of the ADF contrast along the chain in (a) and (b), respectively. Note that the ADF images in (a) and (b) are simultaneously taken when the EELS spectra are gathered and therefore slightly drifted because of the relatively slow scan. Therefore, the line profiles in (c) and (d) were gathered from the ADF images (displayed to the right of the profile), which were taken at the same place just before the EELS analysis in (a) and after the EELS analysis in (b), respectively. The EELS chemical maps are composed from the Cl *L*-edge in (e), the F *K*-edge and Cs *M*-edge in (f), and the O *K*-edge in (g). The experiments were performed at 60 kV. A principal component analysis (PCA) was performed to create the elemental maps in (a) and (b).

images. Here, we show how to use the EELS contrast for the visualisation of these light atoms. Indeed, EELS is greatly advantageous because its contrast does not correspond to the atomic number but is related to the inelastic cross section, which is sufficiently high to discriminate a single light atom such as Li [26]. In addition, the absorption edges detected by EELS are specific for each element and therefore hardly buried in the signals of other neighbouring atoms as long as the target absorption edges are well isolated from the others in the spectra. Furthermore, the spatial resolution of the EELS contrast is normally sufficiently good to resolve individual atoms [27], although EELS signal delocalisation should be considered [28–31].

In this study, we mainly focus on one-dimensional materials, in which various atoms including both heavier and lighter elements are aligned in a row inside a carbon nanotube (Fig. 1). Since the basic structures and properties of the atomic chains are reported in Refs. [26] and [32], we discuss how to characterise non-periodic structures such as vacancies or dopants of light elements in the atomic chain (Fig. 2). We also show the substitution of O atoms in the atomic chains, which has never been reported (Fig. 3). Consequently, light atoms such as K, Cl, O, and F atoms located between heavier atoms, which are in general hardly visible by the ADF contrast and even by the TEM contrast (Fig. 1 and SI), are successfully identified at the single-atom level by the EELS contrast. Furthermore, we also show an example of single Li atom detection (Figs. 4 and 5) adapted from Ref. [26] as the lightest element which we successfully detected as single atoms. Further, we discuss the spatial resolution of EELS contrast images

for single Li atoms.

The microscope used in this study is a JEOL Triple C#1 microscope that consists of a cold FEG (capable of operating at different accelerating voltages of 15, 30, and 60 kV), delta-type Cs correctors for TEM/STEM, and a GATAN quantum GIF spectrometer dedicated to low voltages. The details of the sample preparation for the atomic chains inside the carbon nanotubes or the metallofullerene peapods are described in Ref. [26].

2. Single dopant atoms and mono-vacancies in atomic chains

Fig. 2(a) and (b) show STEM-ADF images of CsI atomic chains inside double-walled carbon nanotubes (DWNTs) [32], both of which show some defective sites. The convergence and collection angles for the ADF imaging are 48 and 79 mrad, respectively (high-angular ADF (HAADF) condition). The specimen was intentionally doped with K and Cl by a vapour-phase method. It is extremely difficult to ascertain the nature of the defects—vacancies or substitutions of other elements—from the ADF images only. Therefore, chemical assignment of these defects by means of EELS is absolutely necessary. Conclusively, the atomic chain in Fig. 2(a) has two defective sites substituted by single K and Cl atoms, while the two defective sites in Fig. 2(b) are expected to be vacancies. Fig. 2(c) and (d) show the elemental map and EELS spectrum taken from the atomic chain in Fig. 2(a). A Cl atom is clearly visible at the I site at the right-side defect in the elemental map constructed from the Cl *L*-edge around ~200 eV (Fig. 2(c) bottom).

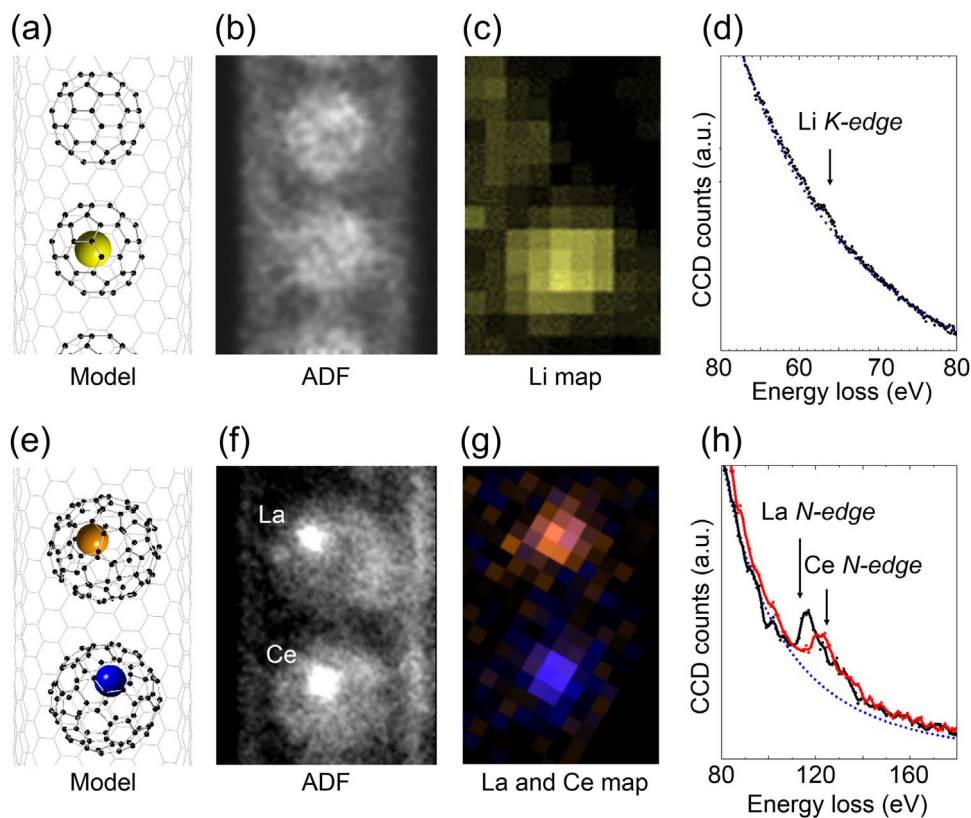


Fig. 4. Detection of a single Li atom in peapods (by STEM operated at 30 kV). (a, b) A model and an ADF image, respectively, for a Li@C₆₀ peapod and (e, f) those for La@C₈₂ and Ce@C₈₂ peapods. In the ADF images, no visible contrast for the Li atom can be seen inside the fullerene cages in (b), while the La and Ce atoms are clearly imaged as bright spots in (f). However, the EELS chemical map in (c) composed by the Li *K-edge* around ~60 eV in (d) indicates the existence of a Li atom in the bottom C₆₀ cage. Compared to the La and Ce EELS chemical maps in (g) composed by the La and Ce *N-edges* around ~120 eV in (h), the Li map seems to be more delocalised because of EELS delocalisation and the atomic movement in which the Li atom inside the cage escapes from the electron beam. The EELS elemental maps in (c) and (g) are smoothed by the convolution of a 3×3 pixel matrix. The images are adapted from Ref. [26] and [34]. Both experiments were performed at 30 kV.

Although the *K* elemental map is quite noisy and it is difficult to extract the *K L-edge* intensity precisely because it just overlaps the *C K-edge*, the maximum of the *K L-edge* intensity extracted by subtraction of *C K-edge* does coincide with a Cs lattice site on the left side. On the other hand, from the vacancy sites in Fig. 2(b), no signal related to possible dopant/impurity atoms was observed under our experimental conditions (Li, O, F, Na, Cl, and K). Note that we cannot completely ignore the possibility of H atoms doped at these defective sites because we still do not have an effective way to detect single H atoms, as discussed later. That is, we cannot distinguish whether this defect is a vacancy or H substitution site, although the latter is unlikely to occur considering the shorter I–H bond length expected, which does not fit the atomic distance observed.

3. Substitution of an O atom at a F site in an atomic chain of CsF

Fig. 3 shows two sequential EELS maps of a CsF atomic chain inside a DWNT. Similar to the case of Cl or K in Fig. 2, a F (*Z*=9) atom is difficult to visualise in the ADF image (Fig. 3(a) (left)). However, the EELS chemical maps taken during the first scan (Fig. 3(a)) clearly show that the trace of a F atom reasonably exists between two Cs atoms to form a CsF chain. Surprisingly, a Cl atom is also found at a F site, which was probably doped unintentionally during the growth process. The Cl impurity is located at the bottom F site. More interestingly, from the second scan (Fig. 3(b)), the upper two F atoms are suddenly substituted with O atoms, and the bottom F atom is simply gone. Consequently, the distance between two Cs atoms is considerably expanded, as shown in the line profiles of the ADF contrast along the chain (Fig. 3(c) and (d)). Although the mechanism of this phenomenon is still unclear, the

following scenario can be assumed: F atoms are basically quite unstable in the presence of the electron beam and tend to be quickly ejected. These ejected F atoms are highly reactive, interact with the surrounding DWNT, and create holes in the walls. Then, O atoms enter through these holes and fill the vacancy sites where the F atoms were initially located. Indeed, O atom insertion into carbon nanotubes was also reported in the case of Eu chains inside a carbon nanotube [33]. The most important implication of the experiment is that simple STEM/TEM imaging is unable to discern which element causes such a phenomenon if no chemical information is available. A simultaneous EELS analysis is indispensable for corroborating unexpected phenomena with unexpected impurities.

4. Single Li-atom detection

Figs. 4 and 5 show the unambiguous detection of individual Li atoms [26]. In Fig. 4, we used the ‘peapod method’, in which individual Li atoms are captured in fullerene cages. This is the standard and most effective approach for capturing single atoms. Commercially available Li@C₆₀ molecules are further encapsulated in a SWNT to form a Li@C₆₀ peapod (Fig. 4(a)). In the ADF image (Fig. 4(b)), the round shape of the C₆₀ molecules inside the SWNT is clearly visible, but no obvious contrast for the Li atoms can be found inside those C₆₀ cages (Fig. 4(b)). However, the EELS chemical map using the Li *K-edge* indicates the presence of Li atoms at the bottom C₆₀ cage (Fig. 4(c)). For comparison, another peapod consisting of La@C₈₂ and Ce@C₈₂ is also shown in Fig. 4(e–h) [34]. In this case, the La and Ce atoms are visible even in the ADF contrast as brighter spots (Fig. 4(f)). The sizes of these brighter spots in ADF image reflect the atomic positions including ‘atomic motion’ such as the thermal vibration or the

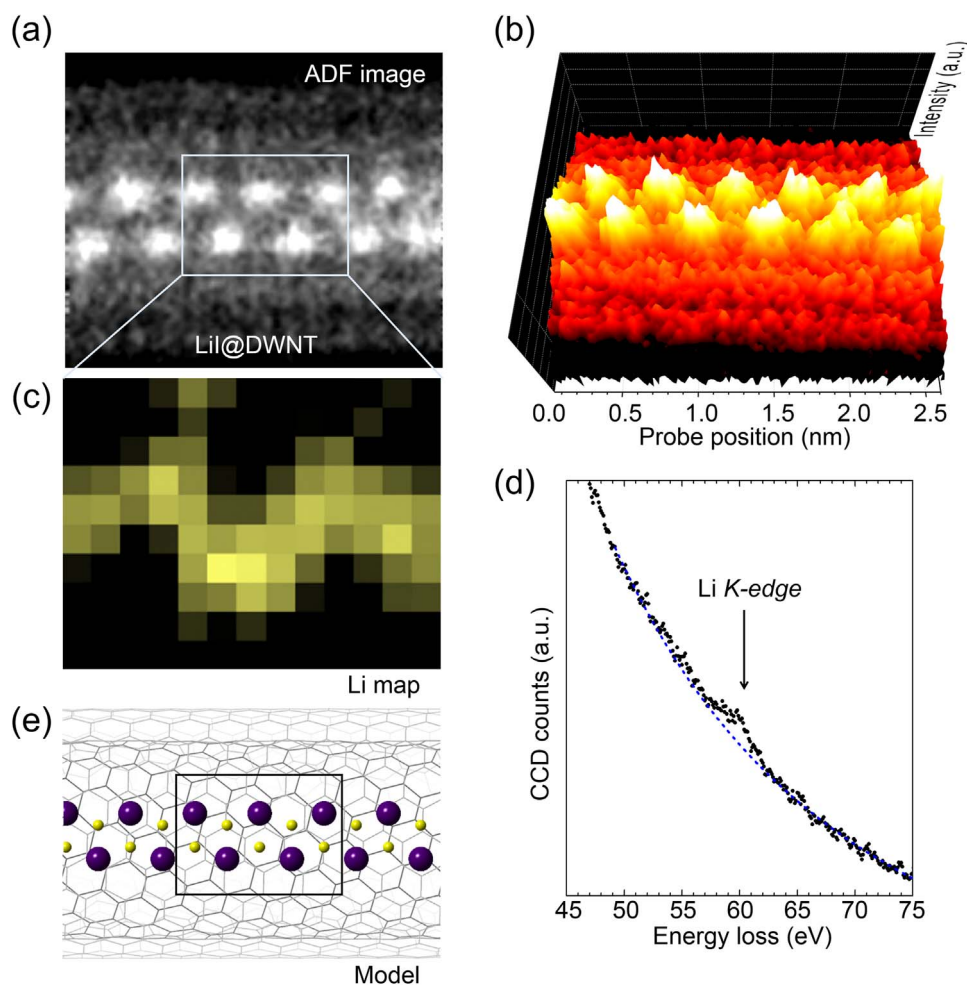


Fig. 5. Detection of Li atoms in a ladder structure of a LiI crystal. (a) ADF image of a ladder structure of a LiI crystal and (b) its contrast intensity map. In the ADF image, only the I atomic positions, which exhibit a zigzag configuration, can be seen. However, the Li chemical map in (c) composed by the Li *K-edge* in (d) obtained from the chain in (a) clearly indicates that the Li atoms are aligned in a zigzag pattern between the I atoms. The expected model of this LiI chain is shown in (e). The EELS elemental map in (c) is smoothed by the convolution of a 3×3 pixel matrix. The images are adapted from Ref. [26]. The experiments were performed at 60 kV.

fluctuation caused by the electron beam as well as ‘the effect of the electron probe tail’. On the other hand, the atomic position displayed in the EELS chemical maps (Fig. 4(g)) further involves ‘the effect of EELS signal delocalisation’ as well as the above two factors. From classical theory, EELS signal delocalisation is inversely proportional to the absorption energy [28]. The expected EELS signal delocalisation for the La and Ce *N-edges* located around 120 eV can be estimated as 0.2 nm at 30 kV. This is the reason why the EELS chemical maps (Fig. 4(g)) indicate that the atomic size is relatively larger than that in the ADF image (Fig. 4(f)) [27]. For the Li case, the atomic position indicated by the EELS chemical map, which is comparable to the size of the fullerene cage, does involve a large EELS signal delocalisation for the Li *K-edge*—estimated as ~0.7 nm at 30 kV—in addition to the atomic motion within the fullerene cage and the effect of electron probe tail. The key to successfully image Li atoms in an EELS chemical map is that the Li atoms are caged so that the Li atom cannot escape, even when the electron beam tries to eject it. It is important to choose the right accelerating voltage to avoid damaging the carbon cage; then, the Li atoms will remain inside the cage, and the e-beam can detect the Li atoms if within the delocalisation distance.

Li atoms can be also trapped in a CNT as a ladder structure of a LiI crystal (Fig. 5). In this case, only I atoms are visible inside the DWNT as brighter spots in the ADF image (Fig. 5(a)). However, the zigzag configuration of I atoms implies the presence of counter ions. Indeed, the alternative zigzag configuration of Li atoms is clearly displayed in the EELS chemical map constructed by using the Li *K-edge* (Fig. 5(c)).

Interestingly, the spatial distribution of the Li signal in this chemical map is much smaller than that for a Li atom inside a C₆₀ molecule in Fig. 4(c). A simple reason for this discrepancy is the difference in the atomic motion. Light elements in atomic chains are more confined (0.4 nm) because of the robust ionic interaction between neighbouring counter ions, while a Li atom inside a C₆₀ molecule moves rather freely in a larger space (0.7 nm). The strong screening effect of the heavier atoms within the atomic chains can be also considered as the reason for the reduction in the delocalisation effect. Such relatively localised EELS signals are advantageous to perceive the location of such invisible light atoms, while a higher spatial resolution for EELS images is needed for a more detailed atomic structural analysis.

In addition, the peak position and shape of the Li *K-edge* vary depending on the atomic configuration or bonding nature; therefore, the chemical states of the Li atoms can be also predicted [26], although the signal obtained from a single Li atom is very weak to discuss the detailed fine structures.

5. Conclusion

We have demonstrated the great potential of atom-by-atom EELS, which can be used to investigate the spatial distributions of individual light atoms such as Li, which are hardly visible in conventional STEM/TEM imaging. Tracking the movements of Li atoms in sequential EELS images will be a great milestone in the near future because it would accelerate some emerging material research such as the development of

electrodes for Li-ion batteries or novel low-dimensional materials doped with light elements.

The detection of single H atoms still remains a challenge. The H *K-edge* appears around ~15 eV, at which large plasmon signals appear and easily hamper the detection of H *K-edge* in such a huge background. In addition, this lightest atom is more likely to escape from the electron beam. Therefore, the detection of single H atoms would not be easily possible unless one could fix them in vacuum. Another possible approach for detection of H atoms which has been recently discussed often is the usage of vibrational spectroscopy [35]. However, this is unfortunately unrealistic for the detection of single H atoms.

Acknowledgements

This work was supported by the Japan Science and Technology Agency (JST) (Grant No. JP16H06333), Research Acceleration Program and the JSPS KAKENHI (Grant Nos. JP26870907, JP25107003).

Appendix A. Supplementary information

Supplementary data associated with this article can be found in the online version at doi:10.1016/j.ultramic.2016.12.007.

References

- [1] A.V. Crewe, J. Wall, J. Langmore, Visibility of single atoms, *Science* 168 (1970) 1338–1340. <http://dx.doi.org/10.1126/science.168.3937.1338>.
- [2] O.L. Krivanek, N. Dellby, A.J. Spence, R.A. Camps, L.M. Brown, Aberration correction in the STEM, in: Proceedings 1997 EMAG Meeting, Institute of Physics Conference Series, vol. 153, 1997, pp. 35–40.
- [3] J. Zach, M. Haider, Aberration correction in a low voltage SEM by a multipole corrector, *Nucl. Instrum. Methods Phys. Res. A* 363 (1995) 316–325. [http://dx.doi.org/10.1016/0168-9002\(95\)00056-9](http://dx.doi.org/10.1016/0168-9002(95)00056-9).
- [4] H. Rose, Outline of a spherically corrected semiplanatic medium-voltage transmission electron-microscope, *Optik* 85 (1990) 19–24.
- [5] M. Haider, G. Braunschhausen, E. Schwan, Correction of the spherical aberration of a 200 kV TEM by means of a Hexapole-corrector, *Optik* 99 (1995) 167–179.
- [6] M. Haider, S. Uhlemann, E. Schwan, H. Rose, B. Kabius, K. Urban, Electron microscopy image enhanced, *Nature* 392 (1998) 768–769. <http://dx.doi.org/10.1038/33823>.
- [7] O.L. Krivanek, N. Dellby, A.R. Lupini, Towards sub-Å electron beams, *Ultramicroscopy* 78 (1999) 1–11. [http://dx.doi.org/10.1016/S0304-3991\(99\)00013-3](http://dx.doi.org/10.1016/S0304-3991(99)00013-3).
- [8] P.E. Batson, N. Dellby, O.L. Krivanek, Sub-angstrom resolution using an aberration corrected electron optics, *Nature* 418 (2002) 617. <http://dx.doi.org/10.1038/nature00972>.
- [9] P.D. Nellist, M.F. Chisholm, N. Dellby, O.L. Krivanek, M.F. Murfitt, Z.S. Szilagy, A.R. Lupini, A. Borisevich, W.H. Sides Jr, S.J. Pennycook, Direct sub-angstrom imaging of a crystal lattice, *Science* 305 (2004) 1741. <http://dx.doi.org/10.1126/science.1100965>.
- [10] M. Isaacson, D. Johnson, The microanalysis of light elements using transmitted energy loss electrons, *Ultramicroscopy* 1 (1975) 33–52. [http://dx.doi.org/10.1016/S0304-3991\(75\)80006-4](http://dx.doi.org/10.1016/S0304-3991(75)80006-4).
- [11] O.L. Krivanek, C. Mory, M. Tence, C. Colliex, EELS quantification near the single-atom detection level, *Microsc. Microanal. Microstruct.* 2 (1991) 257–267. <http://dx.doi.org/10.1051/mm:0199100202-3025700>.
- [12] K. Suenaga, M. Tence, C. Mory, C. Colliex, H. Kato, T. Okazaki, H. Shinohara, K. Hirahara, S. Bandow, S. Iijima, Element-selective single atom imaging, *Science* 290 (2000) 2280–2282. <http://dx.doi.org/10.1126/science.290.5500.2280>.
- [13] K. Kimoto, T. Asaka, T. Nagai, M. Saito, Y. Matsui, K. Ishizuka, Element-selective imaging of atomic columns in a crystal using STEM and EELS, *Nature* 450 (2007) 702–704. <http://dx.doi.org/10.1038/nature06352>.
- [14] D.A. Muller, L.F. Kourkoutis, M. Murfitt, J.H. Song, H.Y. Hwang, J. Silcox, N. Dellby, O.L. Krivanek, Atomic-scale chemical imaging of composition and bonding by, *Science* 319 (2008) 1073–1076. <http://dx.doi.org/10.1126/science.1148820>.
- [15] M. Bosman, V.J. Keast, J.L. Garcia-Munoz, A.J. D'Alfonso, S.D. Findlay, L.J. Allen, Two-dimensional mapping of chemical information at atomic resolution, *Phys. Rev. Lett.* 99 (2007) 86102. <http://dx.doi.org/10.1103/PhysRevLett.99.086102>.
- [16] M. Varela, S.D. Findlay, A.R. Lupini, H.M. Christen, A.Y. Borisevich, N. Dellby, L. Krivanek, P.D. Nellist, M.P. Oxley, L.J. Allen, S.J. Pennycook, Spectroscopic imaging of single atoms within a bulk solid, *Phys. Rev. Lett.* 92 (2004) 95502. <http://dx.doi.org/10.1103/PhysRevLett.92.095502>.
- [17] H. Sawada, T. Sasaki, F. Hosokawa, S. Yuasa, M. Terao, M. Kawazoe, T. Nakamichi, T. Kaneyama, Y. Kondo, K. Kimoto, K. Suenaga, Correction of higher order geometrical aberration by triple 3-fold astigmatism field, *J. Electron Microsc.* 58 (2009) 341–347. <http://dx.doi.org/10.1093/jmicro/dfp033>.
- [18] T. Sasaki, H. Sawada, F. Hosokawa, Y. Kohno, T. Tomita, T. Kaneyama, Y. Kondo, K. Kimoto, Y. Sato, K. Suenaga, Performance of low-voltage STEM/TEM with delta corrector and cold field emission gun, *J. Electron Microsc.* 59 (2010) S7–S13. <http://dx.doi.org/10.1093/jmicro/dfq027>.
- [19] N. Dellby, N.J. Bacon, P. Hrnčirik, M.F. Murfitt, G.S. Skone, Z.S. Szilagy, O.L. Krivanek, Dedicated STEM for 200 to 40 keV operation, *Eur. Phys. J. Appl. Phys.* 54 (2011) 33505. <http://dx.doi.org/10.1051/epjap/201100429>.
- [20] O.L. Krivanek, N. Dellby, M.F. Murfitt, M.F. Chisholm, T.J. Pennycook, K. Suenaga, V. Nicolosi, Gentle STEM: ADF imaging and EELS at low primary energies, *Ultramicroscopy* 110 (2010) 935–945. <http://dx.doi.org/10.1016/j.ultramic.2010.02.007>.
- [21] O.L. Krivanek, M.F. Chisholm, V. Nicolosi, T.J. Pennycook, G.J. Corbin, N. Dellby, M.F. Murfitt, C.S. Own, Z.S. Szilagy, M.P. Oxley, S.T. Pantelides, S.J. Pennycook, Atom-by-atom structural and chemical analysis by annular dark-field electron microscopy, *Nature* 464 (2010) 571–574. <http://dx.doi.org/10.1038/nature08879>.
- [22] K. Suenaga, Y. Sato, Z. Liu, H. Kataura, T. Okazaki, K. Kimoto, H. Sawada, T. Sasaki, K. Omoto, T. Tomita, T. Kaneyama, Y. Kondo, Visualizing and identifying single atoms using electron energy-loss spectroscopy with low accelerating voltage, *Nat. Chem.* 1 (2009) 415–418. <http://dx.doi.org/10.1038/nchem.282>.
- [23] K. Suenaga, M. Koshino, Atom-by-atom spectroscopy at graphene edge, *Nature* 468 (2010) 1088–1090. <http://dx.doi.org/10.1038/nature09664>.
- [24] Y.-C. Lin, P.-Y. Teng, P.-W. Chiu, K. Suenaga, Exploring the single atom spin state by electron spectroscopy, *Phys. Rev. Lett.* 115 (2015) 206803. <http://dx.doi.org/10.1103/PhysRevLett.115.206803>.
- [25] R. Ishikawa, E. Okunishi, H. Sawada, Y. Kondo, F. Hosokawa, E. Abe, Direct imaging of hydrogen-atom columns in a crystal by annular bright-field electron microscopy, *Nat. Mater.* 10 (2011) 278–281. <http://dx.doi.org/10.1038/nmat2957>.
- [26] R. Senga, K. Suenaga, Single-atom electron energy loss spectroscopy of light elements, *Nat. Commun.* 6 (2015) 7943. <http://dx.doi.org/10.1038/ncomms8943>.
- [27] L.H.G. Tizei, Y. Iizumi, T. Okazaki, R. Nakanishi, R. Kitaura, H. Shinohara, K. Suenaga, Single atom spectroscopy: decreased scattering delocalization at high energy losses, effects of atomic movement and X-ray fluorescence yield, *Ultramicroscopy* 160 (2016) 239–246. <http://dx.doi.org/10.1016/j.ultramic.2015.10.019>.
- [28] D. Muller, J. Silcox, Delocalization in inelastic scattering, *Ultramicroscopy* 59 (1995) 195–213. [http://dx.doi.org/10.1016/0304-3991\(95\)00029-Z](http://dx.doi.org/10.1016/0304-3991(95)00029-Z).
- [29] R.F. Egerton, Limits to the spatial, energy and momentum resolution of electron energy-loss spectroscopy, *Ultramicroscopy* 107 (2007) 575–586. <http://dx.doi.org/10.1016/j.ultramic.2006.11.005>.
- [30] W. Zhou, M.P. Oxley, A.R. Lupini, O.L. Krivanek, S.J. Pennycook, J.-C. Idrobo, Single atom microscopy, *Microsc. Microanal.* 18 (2012) 1342–1354. <http://dx.doi.org/10.1017/S1431927612013335>.
- [31] W. Zhou, S.J. Pennycook, J.C. Idrobo, Localization of inelastic electron scattering in the low-loss energy regime, *Ultramicroscopy* 119 (2012) 51–56. <http://dx.doi.org/10.1016/j.ultramic.2011.11.013>.
- [32] R. Senga, H.-P. Komsa, Z. Liu, K. Hirose-Takai, A.V. Krashennnikov, K. Suenaga, Atomic structure and dynamic behaviour of truly one-dimensional ionic chains inside carbon nanotubes, *Nat. Mater.* 13 (2014) 1050–1054. <http://dx.doi.org/10.1038/nmat4069>.
- [33] L.H.G. Tizei, R. Nakanishi, R. Kitaura, H. Shinohara, K. Suenaga, Core-level spectroscopy to probe the oxidation state of single Europium atoms, *Phys. Rev. Lett.* 114 (2015) 197602. <http://dx.doi.org/10.1103/PhysRevLett.114.197602>.
- [34] K. Suenaga, Y. Iizumi, T. Okazaki, Single atom spectroscopy with reduced delocalization effect using a 30 kV-STEM, *Eur. Phys. J. Appl. Phys.* 54 (2011) 33508. <http://dx.doi.org/10.1051/epjap/201100414>.
- [35] O.L. Krivanek, T.C. Lovejoy, N. Dellby, T. Aoki, R.W. Carpenter, P. Rez, E. Soignard, J. Zhu, P.E. Batson, M.J. Lagos, R.F. Egerton, P.A. Crozier, Vibrational spectroscopy in the electron microscope, *Nature* 514 (2014) 209–212. <http://dx.doi.org/10.1038/nature13870>.